Journal of
Polymer Materials

Tech Science Press

https://doi.org/10.32604/jpm.2026.078419

ARTICLE

Structural Amorphization and Ionic Transport Behavior of Phytagel–$NaClO_4$ Biopolymer Electrolytes

Norlela Manja Ahmad[1], **Farisha Irdina Muhammad Ridzuan**[1], **Nur Farisha Sulthan Hussain**[1] and **Siti Zafirah Zainal Abidin**[1,2,*]

[1]Faculty of Applied Sciences, Universiti Teknologi MARA, Shah Alam, Selangor, Malaysia
[2]Ionic Materials and Devices (iMADE) Research Laboratory, Institute of Science, Universiti Teknologi MARA, Shah Alam, Selangor, Malaysia

*Corresponding Author: Siti Zafirah Zainal Abidin. Email: szafirah@uitm.edu.my

Received: 31 December 2025; Accepted: 25 March 2026; Published: 30 June 2026

ABSTRACT: Materials sustainability is becoming increasingly important across advanced technologies, driving the development of environmentally friendly electrolyte systems. In this work, biopolymer electrolytes were prepared using Phytagel as the host polymer and varying concentrations of sodium perchlorate ($NaClO_4$) as the dopant salt via the solution-casting method for sodium-ion battery applications. The prepared biopolymer electrolytes were characterised using various techniques to assess changes in their morphology and electrical performance. X-ray diffraction (XRD) confirms the crystalline/amorphous nature of the prepared biopolymer electrolytes, and the membrane with 40 wt.% NaClO4 exhibits a high degree of amorphousness. Peak-deconvoluted XRD analysis confirms that optimal $NaClO_4$ loading (40 wt.%) induces maximum amorphisation in the Phytagel matrix, minimising crystallite size and crystallinity, thereby establishing a structurally favorable pathway for enhanced ionic conductivity. From electrical analysis, the ionic conductivity calculated for pure phytagel is 2.97×10^{-5} S.cm^{-1}, and on addition of salt, the 40 wt.% of $NaClO_4$ exhibits enhanced ionic conductivity of 2.41×10^{-4} S.cm^{-1} at room temperature. These findings emphasise the importance of optimising salt concentration to achieve an effective balance between structural amorphisation and free-ion availability. This work advances Phytagel-based biopolymer electrolytes as a sustainable and high-performance alternative to conventional polymer electrolytes, offering a viable pathway toward greener battery technologies.

KEYWORDS: Phytagel; sodium perchlorate; biopolymer electrolyte; sodium-ion; structural; electrical

1 Introduction

Rising global energy demand, particularly in renewable and high-technology applications, has accelerated research into advanced energy storage systems. Among these, sodium-ion batteries (SIBs) have emerged as promising alternatives to lithium-ion batteries due to the natural abundance, low cost, and non-toxicity of sodium [1,2]. SIBs exhibit an energy density range of 100–160 Wh·kg^{-1}, making them suitable for large-scale applications, including grid storage and portable electronics. Despite their cost-effectiveness, SIBs still face limitations in achieving long-term stability and high conductivity, as these properties depend strongly on the development of suitable electrolytes [3].

Polymer electrolytes have been extensively studied due to their flexibility, compatibility with electrodes, and ability to provide safe ion transport [4]. More recently, biopolymer electrolytes have attracted increasing attention due to their biodegradability, eco-friendliness, and abundance from renewable resources [5,6].

Unlike synthetic polymers, biopolymers have a lower environmental impact and align with sustainability goals, including SDG 7 (Affordable and Clean Energy) and SDG 12 (Responsible Consumption and Production). However, their application as polymer electrolytes is often limited by inherently low ionic conductivity, arising from restricted polymer chain flexibility and limited ion mobility associated with their semi-crystalline nature [7]. To address this limitation, salt doping is commonly employed to disrupt crystalline domains, increase the amorphous phase, and enhance ionic transport.

In addition to polymer structure, salt characteristics play a crucial role in ion transport. Salts with high lattice energy dissociate poorly, whereas those with lower lattice energy promote greater ion dissociation and increase the concentration of free charge carriers [8]. In this context, sodium perchlorate ($NaClO_4$), owing to its relatively low lattice energy and high solubility, facilitates efficient ionic dissociation, enhances the availability of free Na^+ ions, and further suppresses polymer crystallinity [9]. Meanwhile, Phytagel, a biopolymer derived from Sphingomonas Elodea fermentation, exhibits relatively low crystallinity and structural flexibility, which can be further enhanced by salt doping [10,11]. Therefore, combining Phytagel with $NaClO_4$ offers a promising approach to enhance ionic conductivity and structural stability in biopolymer electrolytes for sodium-ion batteries.

In this work, Phytagel is employed as the host biopolymer while $NaClO_4$ is introduced as a dopant salt to develop sodium-based biopolymer electrolytes. Structural analysis using X-ray Diffraction (XRD) is performed to evaluate changes in crystallinity, while Electrochemical Impedance Spectroscopy (EIS) is used to investigate the ionic conductivity of the prepared electrolyte systems.

2 Experimental Sections

2.1 Materials

Phytagel (Mw: ~500,000 g·mol^{-1}), a high-purity gelling polysaccharide derived from Sphingomonas elodea fermentation, was procured from Sigma-Aldrich (USA). Sodium perchlorate ($NaClO_4$, Mw: 122.44 g·mol^{-1}, ≥98%) was obtained from Merck (Germany) and used as the dopant salt. All chemicals were of analytical grade and used without further purification in the preparation of Phytagel–$NaClO_4$ biopolymer electrolytes.

2.2 Preparation of Biopolymer Electrolytes

Host biopolymer Phytagel (0.5 g) was first dissolved in DMSO with continuous magnetic stirring at 60°C for 12 h, followed by the incorporation of various weight percentages of sodium perchlorate ($NaClO_4$) (ranging from 10 to 50 wt.% in 10 wt.% intervals) and further stirring until a clear solution was formed. The resulting homogeneous solutions were cast into glass Petri dishes and dried in an oven at 60°C for 17 h. The dried polymeric films were then peeled off for subsequent characterization.

2.3 Characterization of Biopolymer Electrolytes

2.3.1 Structural Study

The structural characteristics of the prepared Phytagel–$NaClO_4$ biopolymer electrolyte films were analyzed using X-ray diffraction (XRD) to evaluate their degree of crystallinity and amorphous nature. XRD measurements were carried out using a Bruker AXS diffractometer equipped with CuKα radiation (λ = 1.5418 Å). The diffraction patterns were recorded at room temperature over a 2θ range of 5° to 90°.

2.3.2 Ionic Conductivity Study

The ionic conductivity of the prepared biopolymer electrolytes was evaluated using a HIOKI 3532-50 LCR Hi-Tester over the frequency range of 100 Hz to 1 MHz. The biopolymer electrolyte thin film was sandwiched between two stainless steel current collectors and evaluated at room temperature (300 K). For selected electrolyte compositions, temperature-dependent electrochemical impedance spectroscopy (EIS) measurements were conducted over the temperature range 303–333 K to investigate the influence of temperature on ionic mobility and conductivity. The thickness of the electrolyte films was determined using a digital thickness gauge. The ionic conductivity, σ, of the electrolytes was calculated using the equation:

$$\sigma = \frac{t}{R_b A} \tag{1}$$

where t is the thickness of the electrolyte film, A is the surface contact area (cm^2), and R_b is the bulk resistance obtained from the impedance plot.

2.3.3 Dielectric Study.

The dielectric constant, ε_r, represents the ability of the Phytagel–$NaClO_4$ biopolymer electrolyte to store electrical energy upon polarization under an applied alternating electric field. The real and imaginary components of the dielectric constant were calculated from the impedance data using the equation:

$$\varepsilon_r = \frac{-Z_i}{\omega C_0 \left(Z_r{}^2 + Z_i{}^2\right)} \tag{2}$$

The dielectric loss, ε_i, indicates dielectric loss caused by ion movement and energy dissipation during polarization. It was calculated using the equation:

$$\varepsilon_i = \frac{Z_r}{\omega C_0 \left(Z_r{}^2 + Z_i{}^2\right)} \tag{3}$$

Z_r and Z_i denote the real and imaginary parts of impedance, respectively; $\omega = 2\pi f$ is the angular frequency, and $C_0 = \varepsilon_0$ A/t is the vacuum capacitance. Here, ε_0 is the permittivity of free space (8.854×10^{-12} $F{\cdot}m^{-1}$), A is the electrode area, and t is the thickness of the electrolyte film.

The real modulus, M_r, and M_i were computed using the equations:

$$M_r = \frac{\varepsilon_r}{\left(\varepsilon_r{}^2 + \varepsilon_i{}^2\right)} \tag{4}$$

$$M_i = \frac{\varepsilon_i}{\left(\varepsilon_r{}^2 + \varepsilon_i{}^2\right)} \tag{5}$$

2.3.4 AC Conductivity Study

AC conductivity, σ_{ac}, is one of the most important parameters for interpreting charge transport mechanisms in solid-state materials, particularly polymer electrolytes. The AC conductivity typically follows Jonscher's universal power law, as in the equation:

$$\sigma_{ac}(\omega) = \sigma_{dc} + A\omega^s \tag{6}$$

where ω is the angular frequency, A is a temperature-dependent parameter, s is the power law exponent, and σ_{ac} is the frequency-independent DC conductivity. The exponent's value is determined from the slope of the

linear plot of $ln\ \varepsilon_i$ vs. $ln\ \omega$. By taking the natural logarithm of both sides of the equation, a linearized form is obtained, as expressed in the equation:

$$ln\ \varepsilon_i = -s\ ln\ \omega + ln\ C \tag{7}$$

where s is the exponent of frequencies, which describes the degree of interaction between charge carriers and the lattice.

3 Results and Discussion

3.1 Structural Analysis

Fig. 1 presents the XRD pattern of pure Phytagel powder. A broad diffraction halo is observed in the 2θ range of 15°–25°, with no sharp or well-defined peaks, indicating that Phytagel exhibits predominantly amorphous characteristics despite its semicrystalline nature, as commonly reported for polysaccharide-based biopolymers [12]. The absence of distinct diffraction peaks confirms the lack of long-range crystalline order within the Phytagel matrix. Broad and low-intensity peaks in XRD patterns are typically associated with amorphous structures, which enhance the segmental motion of polymer chains and facilitate ion mobility in polymer electrolytes [13]. This amorphous nature is advantageous for polymer electrolyte applications because amorphous regions promote polymer chain flexibility and support efficient ionic transport. This baseline structural characteristic serves as an important reference for comparison with Phytagel–sodium perchlorate ($NaClO_4$) electrolyte films, which are expected to undergo structural modifications upon salt incorporation.

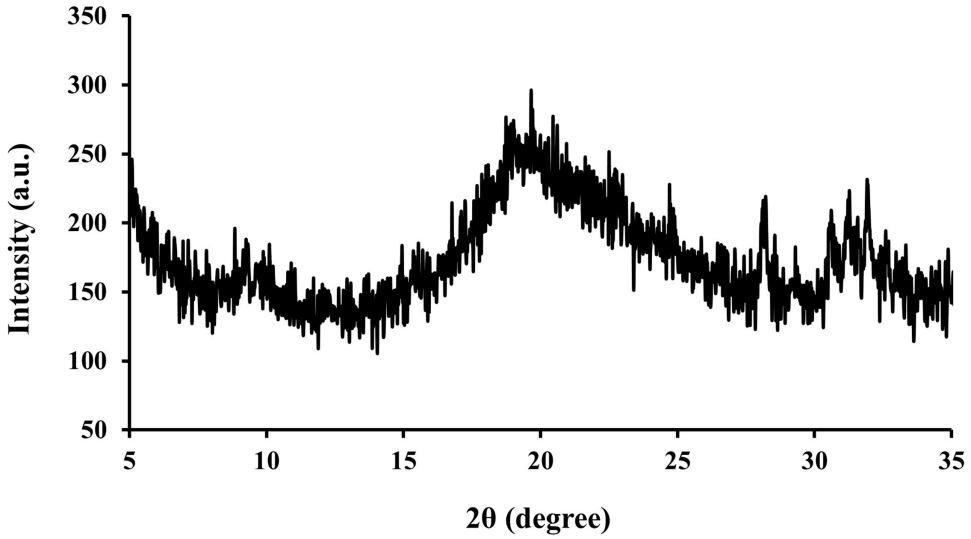

Figure 1: XRD pattern of pure Phytagel biopolymer.

Previous studies have shown that $NaClO_4$ doping significantly alters the structural characteristics of biopolymer electrolytes. In NaCMC-based systems, broad diffraction peaks near 13° and 21° shift or diminish upon the addition of $NaClO_4{\cdot}H_2O$, indicating polymer–salt complexation and the formation of new structural arrangements that reduce crystallinity and enhance ionic conduction [14].

To obtain a clearer understanding of the local structural variations and to quantify the crystalline and amorphous contributions, peak deconvolution was performed on the XRD data. The deconvoluted profiles

(Fig. 2) resolve individual Gaussian components embedded within the broad diffraction envelopes. The salt-free sample (0 wt.%) exhibits a relatively low FWHM value of 1.27, indicating a comparatively higher degree of crystallinity in the Phytagel matrix. Upon incorporation of $NaClO_4$, the FWHM increases significantly, reaching a maximum of 4.50 at 40 wt.% before slightly decreasing to 2.72 at 50 wt.%. In general, a larger FWHM indicates greater amorphous content, which enhances polymer segmental flexibility and promotes ionic conductivity [15]. This trend reflects the progressive disruption of crystalline domains, the emergence of structural disorder, and increased chain mobility. Such an enhanced amorphous environment facilitates ion hopping, thereby improving ionic conductivity [16].

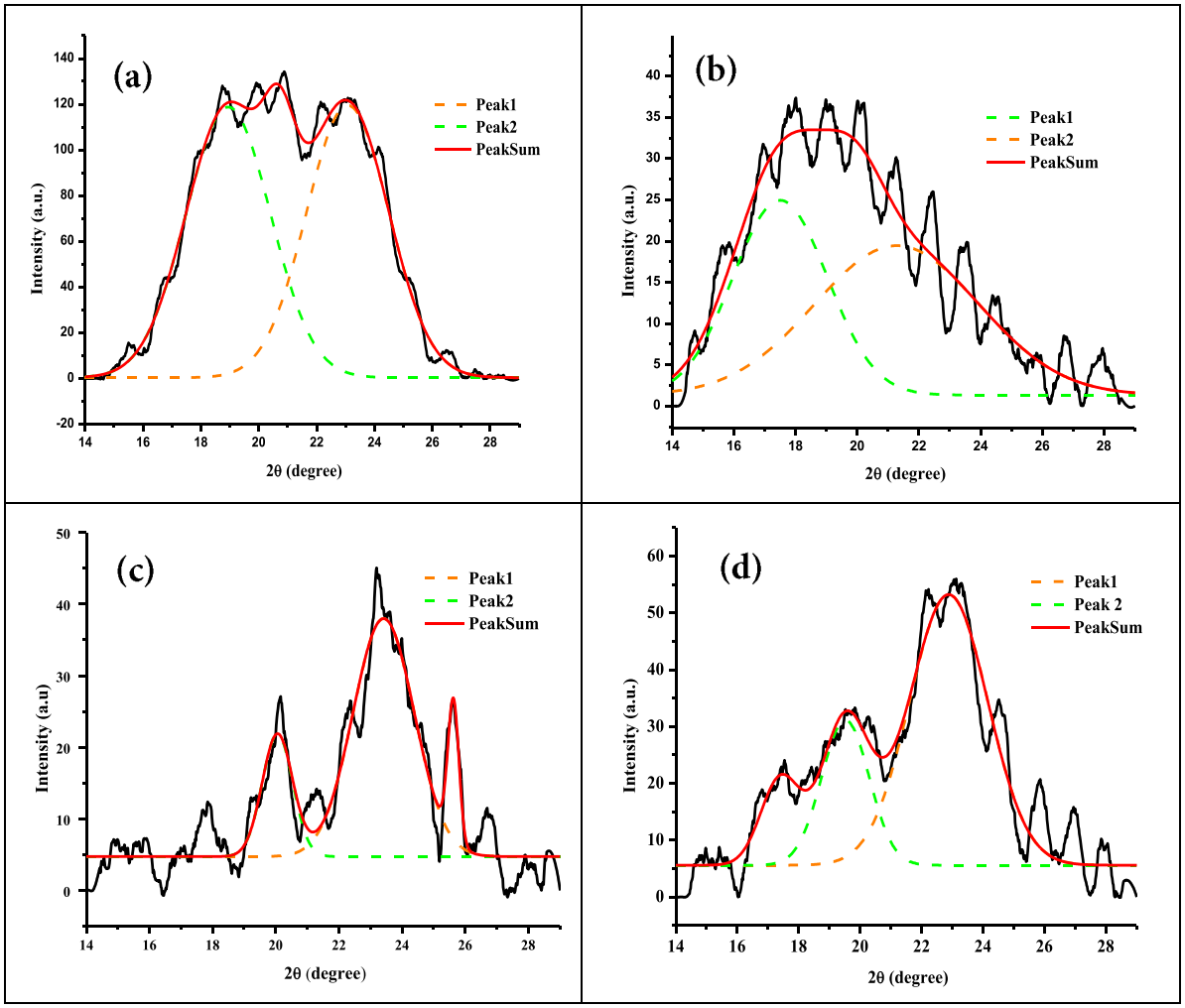

Figure 2: (Continued)

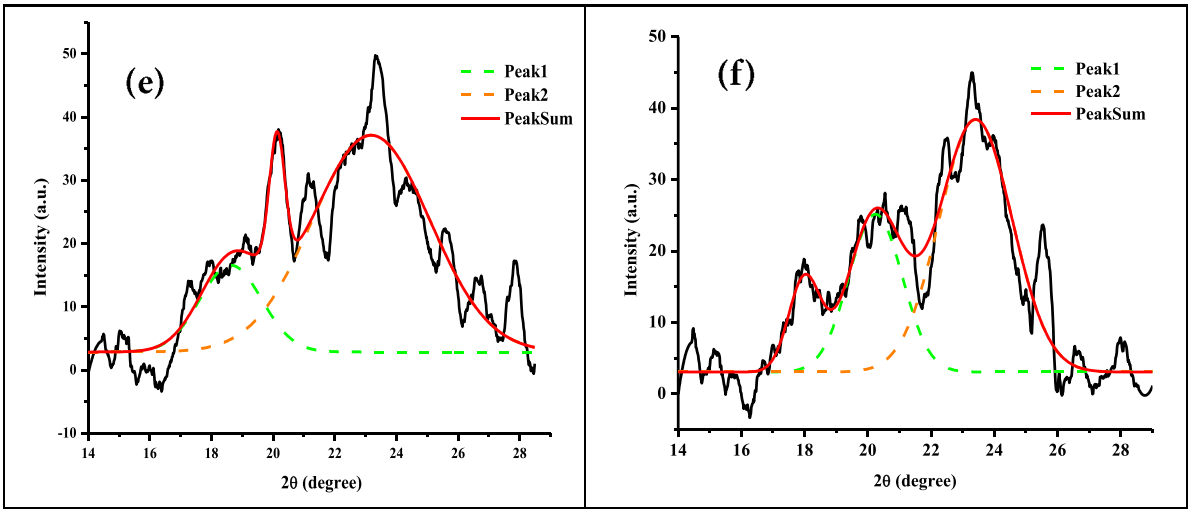

Figure 2: XRD deconvolution of Phytagel-based biopolymer electrolyte containing $NaClO_4$ (**a**) 0 wt.%, (**b**) 10 wt.%, (**c**) 20 wt.%, (**d**) 30 wt.%, (**e**) 40 wt.% and (**f**) 50 wt.%.

Fig. 3a shows that the maximum FWHM at 40 wt.% corresponds to the highest amorphous content in the system, a condition commonly linked to enhanced ionic conductivity. Similar trends have been observed in sodium alginate–$NaClO_4$ electrolytes, where peak broadening was associated with the highest conductivity at ~60 wt.% salt loading [17]. At 50 wt.%, the slight reduction in FWHM may be attributed to ion aggregation or the formation of microcrystalline domains, which restricts further structural disorder. This behavior is consistent with observations in PEO–LiTFSI systems, where amorphous content and conductivity decrease beyond a critical salt concentration due to ionic cluster formation, as indicated by XRD data [17].

Fig. 3b represents the size of the crystallites based on the FWHM values obtained by using the Scherrer equation:

$$L = \frac{0.9\lambda}{FWHM\ \cos\theta} \tag{8}$$

where λ is the X-ray wavelength, which is fixed at 1.5406 Å, and θ is Bragg's diffraction angle.

As anticipated, the crystallite size decreases rapidly with increasing salt concentration, hence, a greater degree of amorphization occurs, down to 18.01 Å at 40 wt.% compared to 63.66 Å at 0 wt.%. However, at 50 wt.%, the crystallite size increases again to 29.86 Å, consistent with partial recrystallization or ion clustering at higher salt content. The negative correlation between FWHM and crystal size indicates a structural transformation in the Phytagel–$NaClO_4$ system and underscores the crucial role of salt concentration in structuring the material to enhance its electrochemical performance.

The degree of crystallinity, X_c, is an essential parameter for determining the structural order of polymer electrolytes, as it strongly influences ionic transport properties. The deconvoluted XRD patterns of all Phytagel–$NaClO_4$ samples were used to calculate the areas corresponding to the crystalline, A_c and amorphous, A_a components. The X_c was then determined from the XRD data using the equation:

$$X_C = \frac{A_c}{A_c + A_a} \times 100\% \tag{9}$$

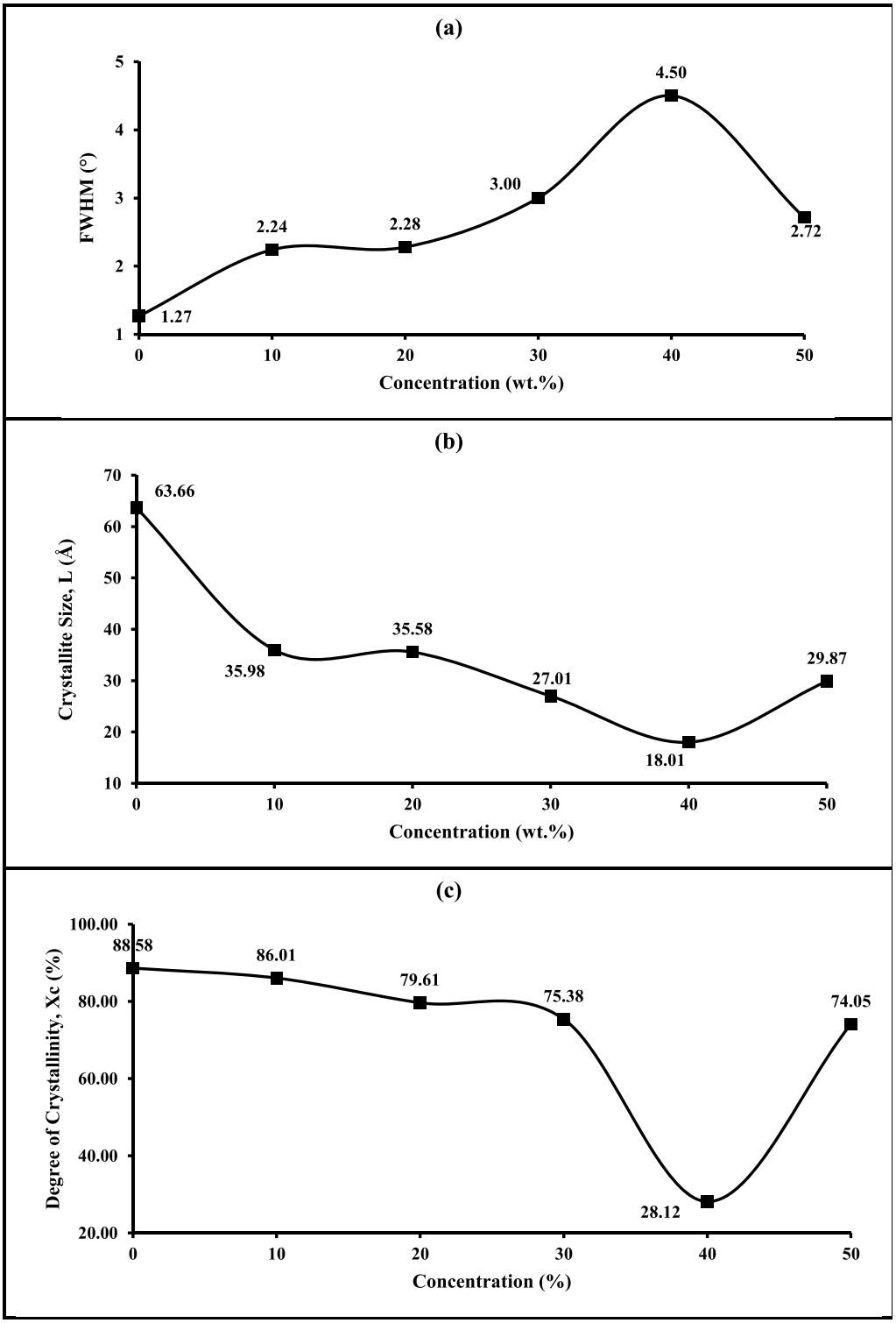

Figure 3: Influence of $NaClO_4$ concentration on the structural parameters of Phytagel-based biopolymer electrolytes, illustrating the variation in (**a**) FWHM, (**b**) crystallite size, and (**c**) degree of crystallinity with the addition of salt (0–50 wt.%).

Table 1 summarizes the peak parameters and the corresponding degree of crystallinity for each composition. As expected, the pure Phytagel sample (0 wt.%) exhibits the highest crystallinity at 88.58%, reflecting its highly ordered structure. The introduction of $NaClO_4$ progressively reduces crystallinity by disrupting the regular packing of polymer chains, thereby enhancing segmental motion and facilitating ion hopping, both of which are essential for improved ionic conductivity.

Table 1: Degree of crystallinity of Phytagel-based biopolymer electrolytes containing different $NaClO_4$ concentrations.

Concentration of $NaClO_4$ (wt.%) Added in Phytagel	Area of the Crystalline Peak, A_c (a.u)	Area of the Amorphous Peak, A_a (a.u)	Degree of Crystallinity, X_c (%)
0	426.69	55.01	88.58
10	121.46	19.75	86.01
20	80.69	20.67	79.61
30	152.15	49.69	75.38
40	13.49	34.49	28.12
50	46.79	16.39	74.05

A slight decrease in crystallinity is observed at 10 wt.% (86.01%), followed by further reductions at higher salt contents, 79.61% at 20 wt.%, 75.38% at 30 wt.%, and a pronounced drop to 28.12% at 40 wt.%. This sharp decline indicates a major structural transition to an amorphous phase, coinciding with the highest ionic conductivity measured in this system. This is consistent with the increase in amorphous fraction and reduction in crystalline domains at this concentration. Interestingly, crystallinity increases again, reaching 74.05% at 50 wt.%, suggesting partial recrystallization or the formation of ionic clusters at high salt loadings. Such clustering can hinder ion mobility and reflect the nonlinear relationship between salt concentration and structural disorder. Fig. 3c illustrates this trend, showing a clear minimum in crystallinity at 40 wt.%, the composition at which effective biopolymer–salt complexation produces the most favorable amorphous structure.

3.2 Ionic Conductivity Analysis

Electrochemical impedance spectroscopy (EIS) was used to evaluate electrical properties, including ionic mobility and interfacial behavior, in the Phytagel–$NaClO_4$ biopolymer electrolytes. The conductivity (Fig. 4) increased from 2.97×10^{-5} S·cm^{-1} at 0 wt.% to a maximum of 2.41×10^{-4} S·cm^{-1} at 40 wt.%, reflecting enhanced $NaClO_4$ dissociation and greater sodium-ion mobility, which is consistent with the reduced crystallinity observed from XRD analysis. At this composition, the bulk resistance was also the lowest, indicating improved charge transport. However, beyond the optimum, the conductivity declined to 2.83×10^{-5} S·cm^{-1} at 50 wt.%. Despite the relatively low crystallinity at this concentration, excessive salt promotes ion aggregation via strong electrostatic interactions, forming neutral ion pairs and clusters that reduce the number of free, mobile ions available for charge transport and, consequently, limit ionic conduction within the polymer matrix [18]. Despite a reduction in conductivity at excessive salt loading, the value remains higher than that of the salt-free system, primarily because dissociated ions remain available to act as charge carriers. The salt-free system, lacking mobile ionic species, exhibits inherently poor ionic conduction. These results show that salt concentration strongly influences ionic conductivity, with 40 wt.% $NaClO_4$ identified as the optimal composition.

Fig. 5 schematically illustrates the mechanism of sodium-ion transport in the phytagel-based biopolymer electrolyte. Upon salt dissolution, sodium perchlorate ($NaClO_4$) dissociates into mobile sodium ions

(Na^+) and perchlorate anions (ClO_4^-). The Na^+ ions coordinate with electron-rich oxygen atoms along the polymer backbone and migrate between coordination sites through a hopping process facilitated by the segmental motion of the polymer chains. Among the available functional groups, the negatively charged carboxylate ($-COO^-$) provides strong electrostatic interactions and likely serves as the primary coordination center, while ether and hydroxyl oxygens act as secondary pathways for ion transport. The high density of oxygen-containing groups in phytagel provides abundant coordination sites, and the incorporation of $NaClO_4$ enhances ionic conductivity by increasing the charge-carrier concentration and promoting effective salt dissociation within the polymer matrix.

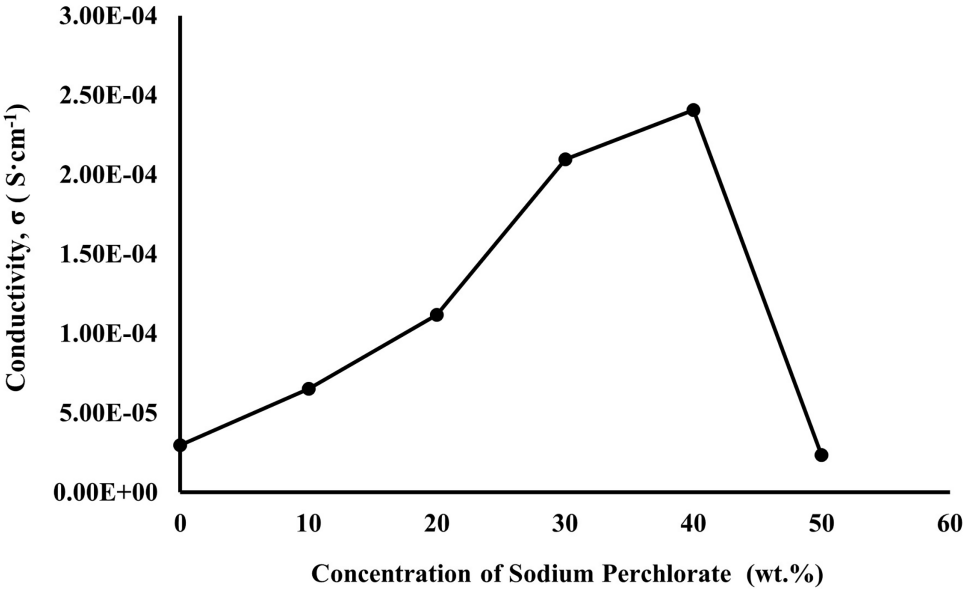

Figure 4: Room-temperature ionic conductivity of Phytagel–$NaClO_4$ biopolymer electrolytes at salt concentrations of 0, 20, 30, 40, and 50 wt.%.

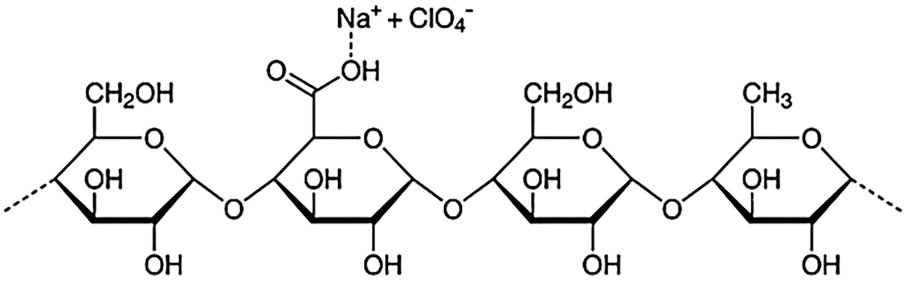

Figure 5: Mechanism of ionic conduction of $NaClO_4$-Phytagel.

Following the concentration-dependent conductivity analysis, the influence of temperature on ionic transport in the Phytagel–$NaClO_4$ biopolymer electrolytes was further investigated. Temperature plays a crucial role in governing ionic conductivity in biopolymer electrolyte systems, as it directly influences ion mobility and polymer chain dynamics. Polymer hosts are typically semicrystalline, comprising crystalline and amorphous regions, with the latter providing the primary pathway for ion transport due to its greater structural disorder and chain flexibility. As temperature increases, thermal energy promotes the expansion of these amorphous domains, thereby creating a more favorable environment for ionic conduction [19,20].

However, a slight initial decrease in conductivity was observed, which may be attributed to transient ion association and localized polymer-chain rearrangements that temporarily restrict charge-carrier mobility. With further increases in temperature, increased thermal energy facilitates polymer segmental motion and promotes ion dissociation, thereby increasing the population of free ions available for conduction. Consequently, all samples exhibit thermally activated transport behavior, as evidenced by the overall increase in conductivity with temperature, as summarized in Table 2.

Table 2: Temperature dependence of ionic conductivity for Phytagel–$NaClO_4$ biopolymer electrolytes with salt contents of 0, 40, and 50 wt.% measured by electrochemical impedance spectroscopy.

Temperature (K)	Conductivity 0 wt.% $NaClO_4$, σ ($S.cm^{-1}$)	Conductivity 40 wt.% $NaClO_4$, σ ($S.cm^{-1}$)	Conductivity 50 wt.% $NaClO_4$, σ ($S.cm^{-1}$)
303	5.67×10^{-5}	1.82×10^{-4}	6.05×10^{-4}
313	6.26×10^{-5}	1.60×10^{-4}	3.18×10^{-4}
323	3.50×10^{-4}	1.48×10^{-4}	2.14×10^{-4}
333	6.70×10^{-4}	2.11×10^{-3}	5.73×10^{-3}

Accordingly, conductivity measurements were carried out over the temperature range of 303–333 K for electrolytes containing 0, 40, and 50 wt.% $NaClO_4$. Interestingly, the 50 wt.% electrolyte exhibited a pronounced increase in conductivity from the 10^{-5} to 10^{-4} $S{\cdot}cm^{-1}$ range with a slight temperature rise from 300 to 303 K, which can be attributed to thermally activated ion transport consistent with Arrhenius-type behavior. As temperature increases, enhanced segmental motion of the polymer chains generates greater free volume, facilitating ion hopping between coordination sites and thereby improving ionic conductivity [21]. Similar behavior has been reported in agarose-based biopolymer electrolytes, where increased chain flexibility at elevated temperatures promotes ion transport [22].

Among the investigated compositions, the electrolyte containing 40 wt.% $NaClO_4$ demonstrates the highest ionic conductivity, reaching a maximum value of 2.11×10^{-3} $S{\cdot}cm^{-1}$ at 333 K. This result indicates that ion transport is most efficient at this optimal salt concentration due to enhanced amorphous content and increased availability of mobile charge carriers. In contrast, the salt-free electrolyte (0 wt.%) exhibits the lowest conductivity over the temperature range due to the absence of mobile sodium ions. Although the 50 wt.% $NaClO_4$ shows higher conductivity than the salt-free system; however, its performance remains inferior to that of the 40 wt.% sample, likely due to ion aggregation and reduced ion mobility at excessive salt loading. These findings confirm that an optimal salt concentration is necessary to balance charge-carrier density and polymer segmental motion for efficient ionic transport.

3.3 Dielectric Studies

Fig. 6 illustrates the frequency dependence of the dielectric constant of the Phytagel–sodium perchlorate biopolymer electrolyte at different temperatures (303–333 K). As shown in Fig. 6, ε_r exhibits very high values at low frequencies, particularly at 323 K, which is attributed to the accumulation of mobile Na^+ ions at the electrode–electrolyte interface, resulting in strong interfacial (space-charge) polarization. With increasing frequency, ε_r decreases sharply because ions and dipoles cannot follow the rapidly oscillating electric field, thereby reducing polarization [23]. In addition, ε_r increases with temperature due to enhanced segmental motion of polymer chains and increased ionic mobility, peaking at 323 K, indicating optimal conditions for ionic transport.

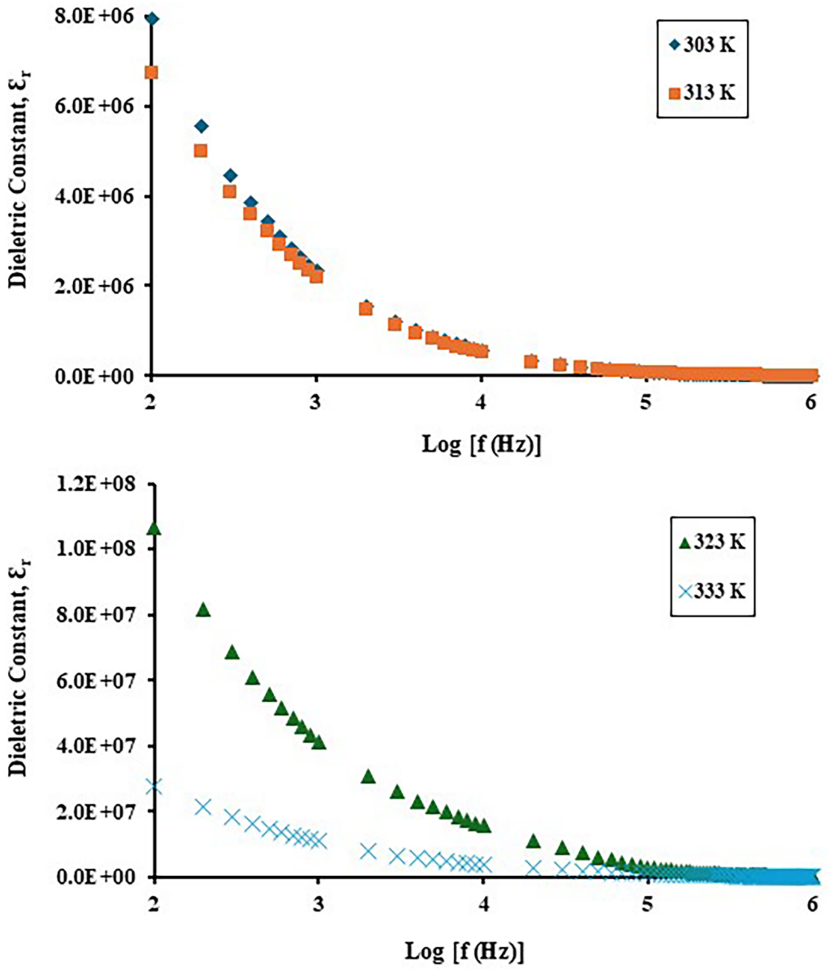

Figure 6: Temperature dependence of the dielectric constant for Phytagel-based biopolymer electrolyte containing 40 wt.% $NaClO_4$ in the temperature range of 300–333 K.

Fig. 7 shows the variation of the dielectric constant with frequency at different temperatures. Higher ε_i values are observed at low frequencies, particularly at 323 and 333 K, indicating increased dielectric loss due to ion accumulation at the electrode–electrolyte interface. As frequency increases, ε_i decreases markedly because the ions cannot respond to the rapidly changing electric field, thereby reducing energy dissipation. The increase in ε_i with temperature in the low-frequency region reflects enhanced ionic mobility and polymer chain flexibility. The highest ε_i values at 323 K suggest stronger ion–polymer interactions and more effective ionic motion within the electrolyte system.

The results indicate that the dielectric constant and dielectric loss of this biopolymer electrolyte system are strongly dependent on both frequency and temperature. At low frequencies and elevated temperatures, interfacial polarization and ionic motion dominate the dielectric response of the system. The observed non-Debye relaxation behaviour, together with the enhanced values of ε_r and ε_i at 323 K, confirms the significant role of thermal activation and ion-hopping mechanisms in governing the dielectric properties of the phytagel–$NaClO_4$ biopolymer electrolyte.

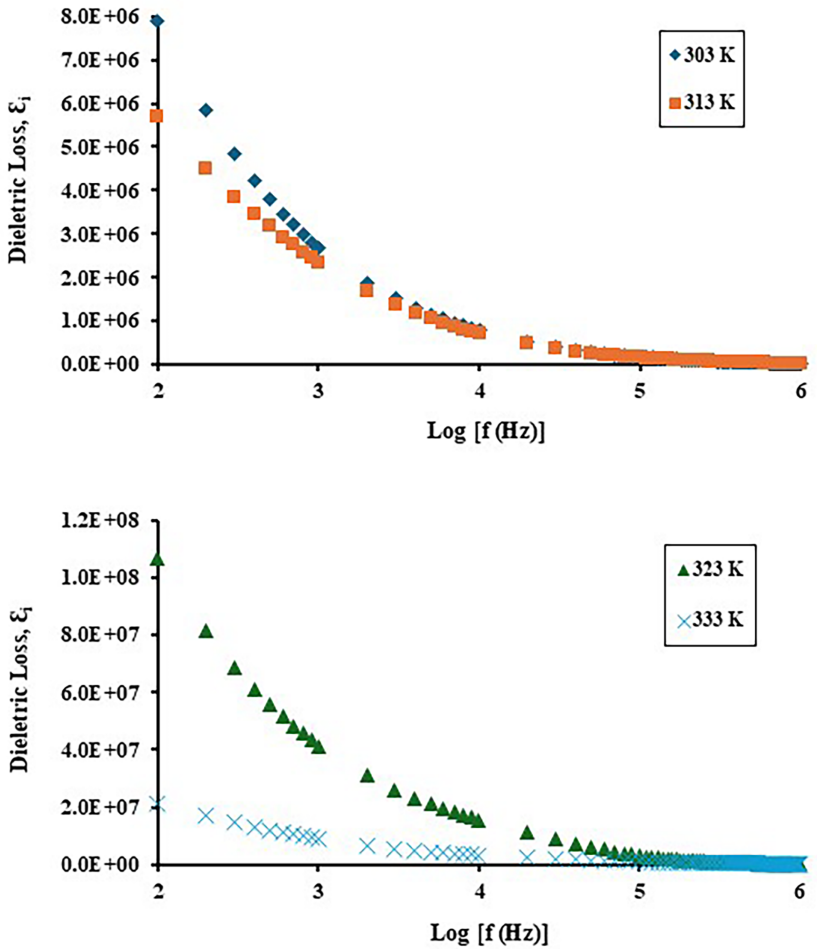

Figure 7: Temperature dependence of the dielectric loss for Phytagel-based biopolymer electrolyte containing 40 wt.% $NaClO_4$ in the temperature range of 300–333 K.

Fig. 8 illustrates the frequency dependence of the real part of the modulus. The M_r values remain relatively low across the frequency range, particularly at lower frequencies, a characteristic of materials with high dielectric permittivity and indicative of the dominance of electrode polarization effects. As the frequency increases beyond log f ≈ 4.5, M_r begins to rise due to the reduction of space-charge polarization and the emergence of bulk relaxation processes. The enhancement in M_r is more pronounced at 313 K, suggesting improved segmental motion of the polymer chains that facilitates ion migration. At higher temperatures (323 and 333 K), the M_r curves exhibit gentler slopes, possibly indicating more homogeneous ionic relaxation behavior resulting from increased thermal activation.

Fig. 9 presents the frequency dependence of the imaginary part of the modulus. At low frequencies (log f < 4.0), the M_i values are nearly temperature-independent and approach zero, implying negligible electrode polarization effects and the dominance of long-range ion transport. With further increases in frequency, a sharp rise in M_i is observed, marking the onset of dielectric relaxation as ions begin to hop between coordination sites. The most prominent increase in M_i occurs at 313 K, where a sharp upward trend is evident around log f ≈ 5.0, indicating a reduced relaxation time and enhanced ionic mobility. At elevated temperatures (323 and 333 K), the increase in M_i shifts toward slightly lower frequencies, reflecting the thermally activated nature of the relaxation process.

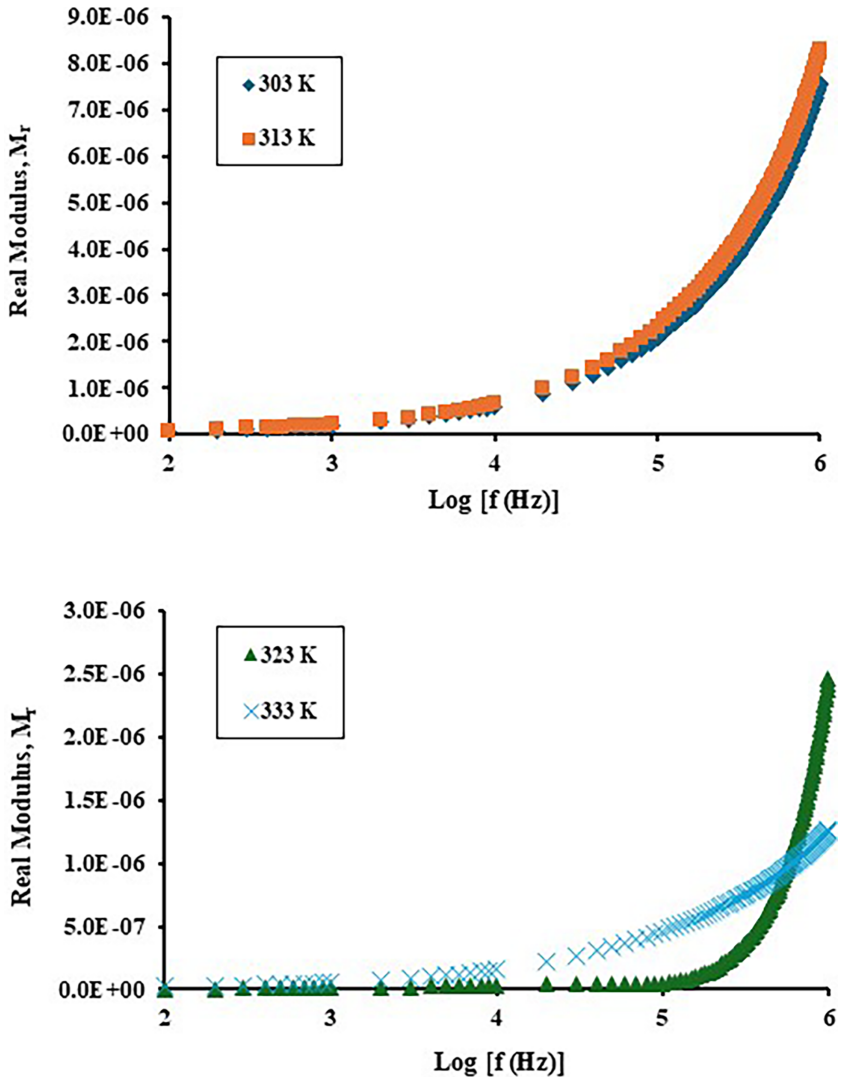

Figure 8: Temperature dependence of the real part of the modulus for Phytagel-based biopolymer electrolyte containing 40 wt.% of $NaClO_4$ in the temperature range of 300–333 K.

The results indicate that the M_r and M_i analyses reveal strongly thermally activated ionic conductivity at 40 wt.% Phytagel–sodium perchlorate system. The temperature-induced shift of the frequency-dependent M_i response toward lower frequencies, together with the increase in M_r, demonstrates that higher thermal energy enhances ion dynamics by promoting ion hopping and polymer segmental mobility. These observations confirm that ionic transport in this system proceeds predominantly through a thermally assisted hopping mechanism and is strongly governed by polymer chain flexibility and temperature.

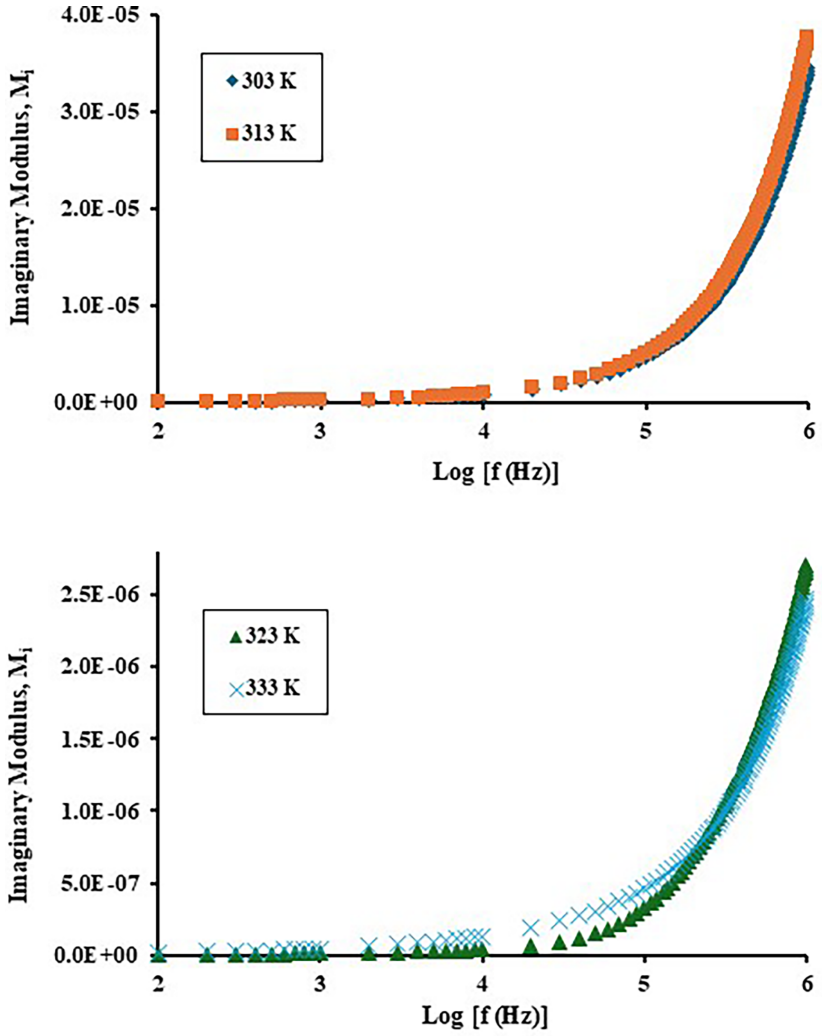

Figure 9: Temperature dependence of the imaginary part of the modulus for Phytagel-based biopolymer electrolyte containing 40 wt.% of $NaClO_4$ in the temperature range of 300–333 K.

3.4 AC Conductivity Analysis

Fig. 10 shows the AC conductivity, $\sigma_{ac,}$ of the samples measured over the frequency range 100 Hz to 1 MHz at four temperatures (303, 313, 323, and 333 K). At all temperatures, σ_{ac} increases with frequency, particularly in the high-frequency region, which is consistent with a hopping-based conduction mechanism. The conductivity is also thermally activated, increasing with temperature. Notably, at 323 K, a relaxation anomaly is observed in the frequency range of log f ≈ 4.6–5.0. Similar features have been attributed to electrode polarization and Maxwell–Wagner–Sillars (MWS) interfacial polarization effects in systems with porous electrodes [24] and nanocomposite oxides [25]. In addition, electrode polarization is often associated with a reduced conductivity exponent and the appearance of conductivity dips, as reported in dielectric studies of perovskite materials [26]. These observations suggest that the anomaly originates from interfacial charge dynamics, which are likely responsible for the observed decrease in σ_{ac}.

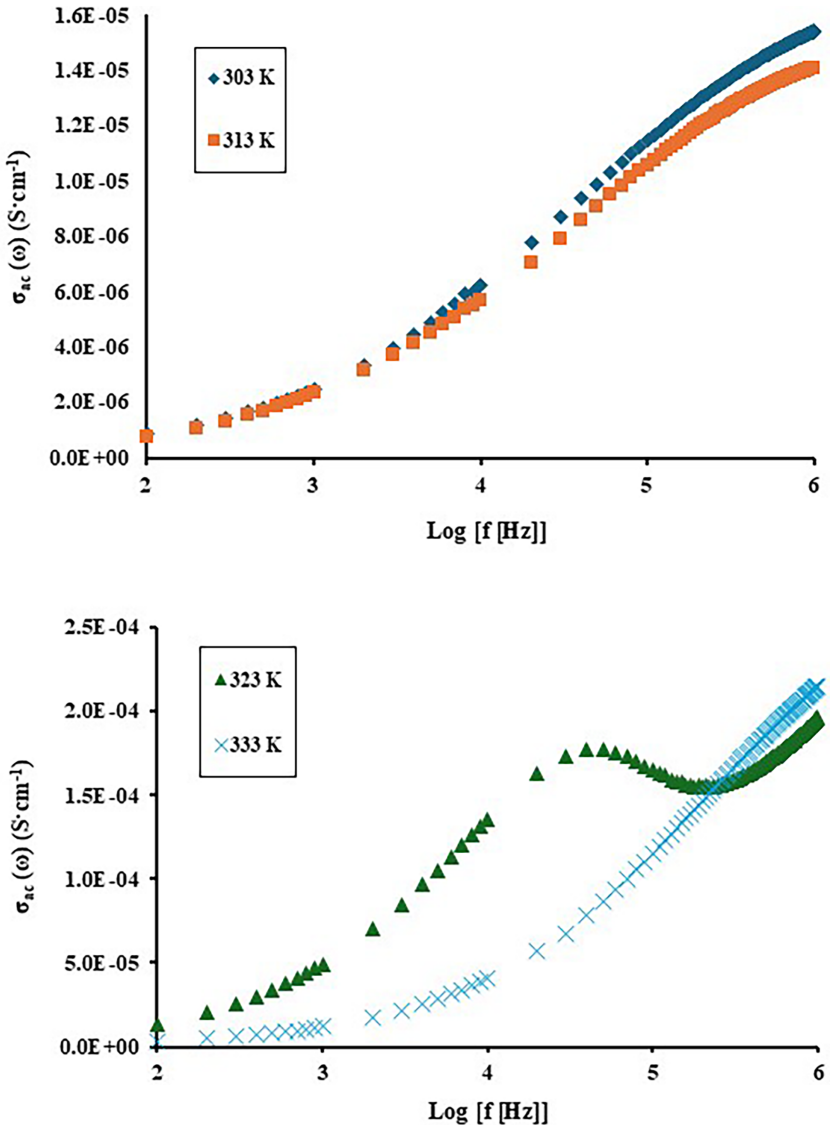

Figure 10: Frequency-dependent AC ionic conductivity of Phytagel-based biopolymer electrolyte containing 40 wt.% of $NaClO_4$ in the temperature range of 300–333 K.

Fig. 11 presents the ln ε_i vs. ln ω plots for the Phytagel–$NaClO_4$ biopolymer electrolyte at temperatures between 300 and 333 K. The plots exhibit good linearity, indicating power-law behavior characteristic of dielectric relaxation in disordered polymer systems. The slope decreases with increasing temperature, from −0.667 at 300 K to −0.406 at 323 K, suggesting that dielectric loss becomes less frequency-dependent as thermal energy increases ionic mobility and polymer segmental flexibility. This behavior is consistent with non-Debye relaxation and Jonscher's universal dielectric response reported for solid polymer electrolytes, in which charge-carrier hopping and interfacial polarization dominate the dielectric response [27].

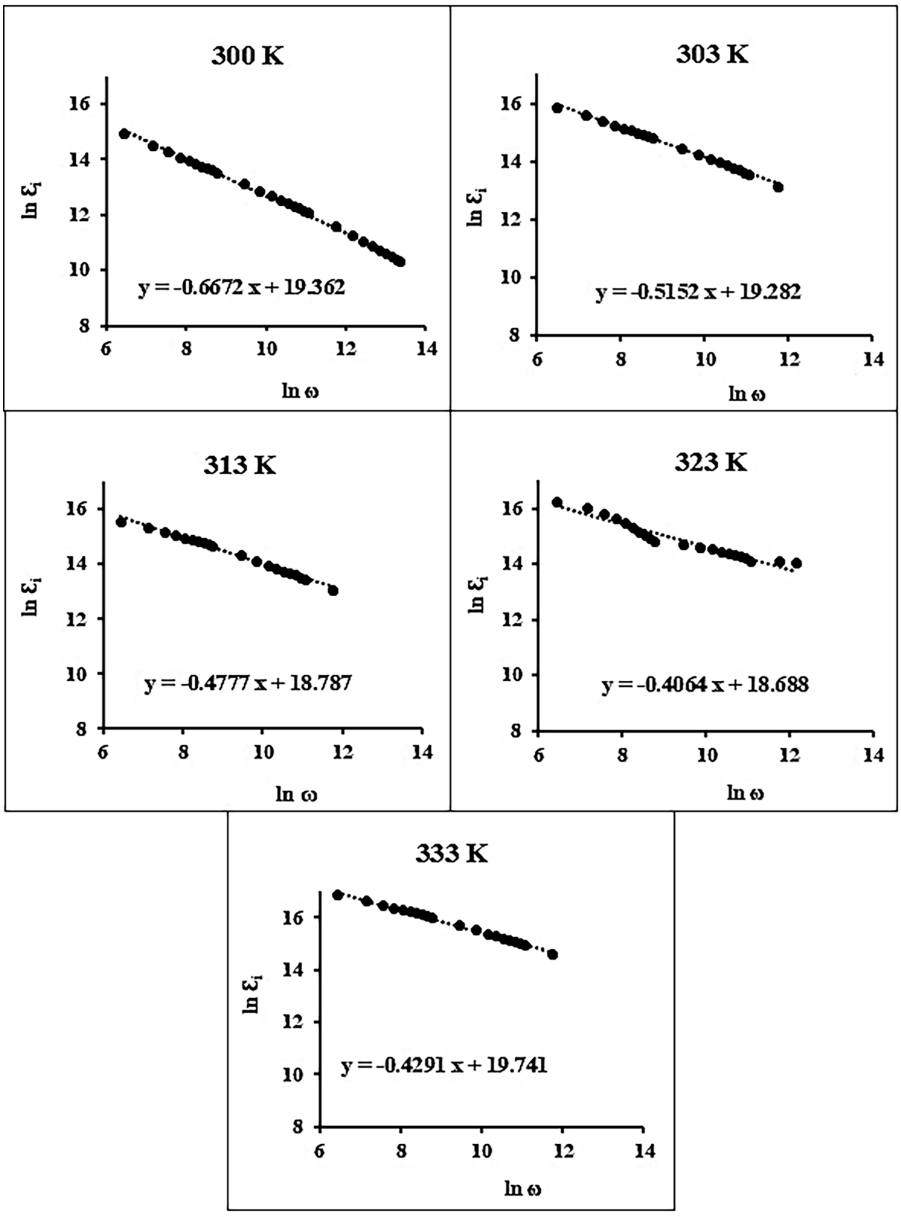

Figure 11: ln ε_i vs. ln ω of Phytagel-based biopolymer electrolyte containing 40 wt.% of $NaClO_4$ in the temperature range of 300–333 K.

From the linear fits, the power-law exponent s was extracted and plotted as a function of temperature (Fig. 12). The obtained s values indicate a thermally assisted hopping process, with lower s values corresponding to long-range ionic transport within the electrolyte matrix. Based on Fig. 10, the power-law exponent exhibits an explicit temperature dependence, increasing from 0.3328 at 300 K to a maximum value of 0.5936 at 323 K. This temperature-induced increase in s is consistent with the Correlated Barrier Hopping (CBH) model, which describes ion transport in highly disordered polymer systems as a thermally activated hopping process between localized sites [28]. The rise in s reflects enhanced polymer segmental mobility and reduced effective energy barriers for ion hopping as temperature increases. A slight decrease in s at 333 K suggests the onset of ionic aggregation or clustering, which may restrict high-frequency charge transport and limit ionic

mobility. Similar behavior has been reported in molecular dynamics simulations, in which increased thermal energy at elevated temperatures promotes ion aggregation and reduces ion diffusivity [29]. Overall, the temperature dependence of s confirms that ionic conduction in the Phytagel–$NaClO_4$ biopolymer electrolyte follows the CBH mechanism within the investigated temperature range. It is also worth noting that, although the structural and electrical properties of gellan gum (Phytagel)-based $NaClO_4$ biopolymer electrolytes have been previously reported [30], the present work places greater emphasis on systematically correlating structural parameters with ionic transport behavior.

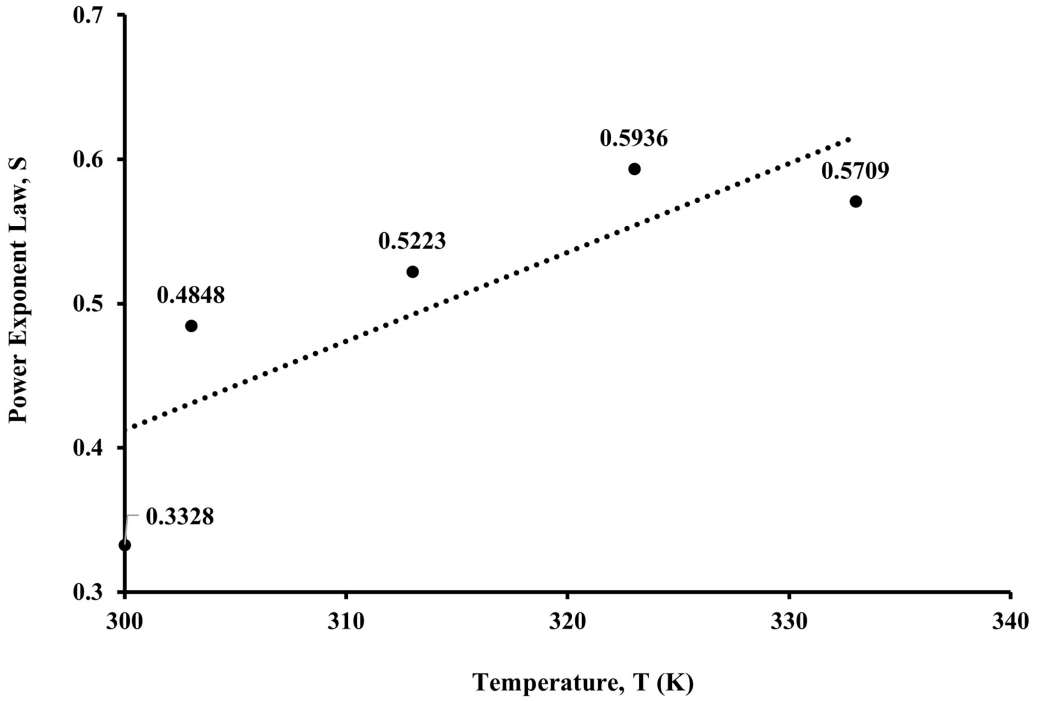

Figure 12: Power exponent law of a Phytagel-based biopolymer electrolyte containing 40 wt.% of sodium perchlorate at different temperatures.

4 Conclusion

Phytagel–$NaClO_4$ biopolymer electrolytes with salt concentrations ranging from 0 to 50 wt.% were successfully prepared by solution casting and systematically characterised using XRD and EIS. Structural analysis revealed that $NaClO_4$ incorporation progressively disrupted the crystalline domains of Phytagel, with the highest amorphous content achieved at 40 wt.% salt loading, as evidenced by peak broadening, increased FWHM, reduced crystallite size, and a significant decrease in crystallinity. This enhanced amorphisation directly correlated with improved ionic conductivity. Electrical measurements showed that the ionic conductivity increased with salt concentration, reaching a maximum at 40 wt.% $NaClO_4$. Dielectric and modulus analyses further confirmed non-Debye relaxation behavior, strong interfacial polarisation, and thermally assisted ion hopping mechanisms, particularly at the optimal salt composition. Overall, the results demonstrate that 40 wt.% $NaClO_4$ provides the optimal balance between structural disorder and ionic mobility, underscoring the strong potential of Phytagel–$NaClO_4$ biopolymer electrolytes for sodium-based sustainable energy storage applications.

Acknowledgement: The authors would like to thank the iMADE Research Laboratory, the Institute of Science, and the Faculty of Applied Sciences, Universiti Teknologi MARA (UiTM), for providing research facilities to carry out this project.

Funding Statement: The authors received no specific funding for this study.

Author Contributions: All authors contributed substantially in accordance with the journal's authorship criteria. Norlela Manja Ahmad performed the sample preparation and characterizations, data validation, and analysis. Farisha Irdina Muhammad Ridzuan contributed to manuscript editing, organization, technical review, and language refinement. Nur Farisha Sulthan Hussain provided technical guidance on instrument operation and experimental procedures. Siti Zafirah Zainal Abidin conceptualized the research, supervised the experimental design, and contributed to data interpretation. All authors reviewed and approved the final version of the manuscript.

Availability of Data and Materials: The data and code that support the findings of this study are available from the corresponding author upon reasonable request.

Ethics Approval: Not applicable.

Conflicts of Interest: The authors declare no conflicts of interest.

References

1. Hu F, Lin H, Pan R. Feasibility analysis of replacing lithium-ion battery with sodium ion battery. Highlights Sci Eng Technol. 2024;90:81–6. doi:10.54097/x8wyc672.
2. Gao Y, Zhang H, Peng J, Li L, Xiao Y, Li L, et al. A 30-year overview of sodium-ion batteries. Carbon Energy. 2024;6(6):e464. doi:10.1002/cey2.464.
3. Phogat P, Dey S, Wan M. Comprehensive review of sodium-ion batteries: principles, materials, performance, challenges, and future perspectives. Mater Sci Eng B. 2025;312(3):117870. doi:10.1016/j.mseb.2024.117870.
4. Kamali-Heidari E, Kamyabi-Gol A, Heydarzadeh Sohi M, Ataie A. Electrode materials for lithium ion batteries: a review. J Ultrafine Grained Nanostructured Mater. 2018;51(1):1–12. doi:10.22059/JUFGNSM.2018.01.01.
5. Aziz SB, Brevik I, Hamsan MH, Brza MA, Nofal M, Abdullah M, et al. Compatible solid polymer electrolyte based on methyl cellulose for energy storage application: structural, electrical, and electrochemical properties. Polymers. 2020;12(10):2257. doi:10.3390/polym12102257.
6. Mejenom AA, Muthiah M, Mohamad Isa MIN. Ionic conductivity studies on proton conducting solid biopolymer electrolyte based on 2-hydroxyethyl cellulose (2HEC) doped with ammonium chloride (NH4CL). J Adv Res Fluid Mech Therm Sci. 2024;121(2):147–58. doi:10.37934/arfmts.121.2.147158.
7. Al-Rafai H, Khalil KD, Bashal AH, Alotaibi AA, Alarifi N, Alharbi AF, et al. Revolutionizing dielectric and electrical properties of carboxymethylcellulose/ZnO nanocomposites: a detailed exploration of experimental findings and computational insights for advanced material engineering. Int J Biol Macromol. 2025;308(Pt 2):142406. doi:10.1016/j.ijbiomac.2025.142406.
8. O'Donnell LF, Greenbaum SG. Review of multivalent metal ion transport in inorganic and solid polymer electrolytes. Batteries. 2021;7(1):3. doi:10.3390/batteries7010003.
9. Abdul Manap NR, Shamsudin I, Shrgawi N, Kasim N, Noor A, Taufik S, et al. Effect of $NaClO_4$ dopant on chemical bond and ionic conductivity of benzoyl kappa-carrageenan gel biopolymer electrolyte. Res Sq. 2023;77(2):1–16. doi:10.21203/rs.3.rs-3191191/v1.
10. Karuppasamy K, Prasanna K, Ilango PR, Vikraman D, Bose R, Alfantazi A, et al. Biopolymer phytagel-derived porous nanocarbon as efficient electrode material for high-performance symmetric solid-state supercapacitors. J Ind Eng Chem. 2019;80:258–64. doi:10.1016/j.jiec.2019.08.003.
11. Cardoso MB, Bodanese-Zanettini MH, de Mundstock EC, Kaltchuk-Santos E. Evaluation of gelling agents on anther culture: response of two soybean cultivars. Braz Arch Biol Technol. 2007;50(6):933–9. doi:10.1590/s1516-89132007000700004.

12. Kumar S, Singh MK, Savilov SV, Yahya MZA, Singh PK. Ion dynamics and electrochemical performance of biopolymer phytagel and sodium thiocyanate-blended solid polymer electrolytes. Ionics. 2025;31(1):439–51. doi:10.1007/s11581-024-05878-7.
13. Nayak P, Sudhakar YN, De S, Ismayil, Shetty SK. Optimization of chitosan: methylcellulose polyblend to obtain highly amorphous polymer matrix useful for ion transportation. Indian J Phys. 2023;97(12):3483–93. doi:10.1007/s12648-023-02684-1.
14. Shetty SK, Ismayil, Noor IM. Effect of new crystalline phase on the ionic conduction properties of sodium perchlorate salt doped carboxymethyl cellulose biopolymer electrolyte films. J Polym Res. 2021;28(11):415. doi:10.1007/s10965-021-02781-x.
15. Li Z, Fu J, Zhou X, Gui S, Wei L, Yang H, et al. Ionic conduction in polymer-based solid electrolytes. Adv Sci. 2023;10(10):2201718. doi:10.1002/advs.202201718.
16. Polu AR, Singh PK. Improved ion dissociation and amorphous region of PEO based solid polymer electrolyte by incorporating tetracyanoethylene. Mater Today Proc. 2022;49:3093–7. doi:10.1016/j.matpr.2020.10.950.
17. Iwaki YO, Escalona MH, Briones JR, Pawlicka A. Sodium alginate-based ionic conducting membranes. Mol Cryst Liq Cryst. 2012;554(1):221–31. doi:10.1080/15421406.2012.634329.
18. Bakar R, Darvishi S, Aydemir U, Yahsi U, Tav C, Menceloglu YZ, et al. Decoding polymer architecture effect on ion clustering, chain dynamics, and ionic conductivity in polymer electrolytes. ACS Appl Energy Mater. 2023;6(7):4053–64. doi:10.1021/acsaem.3c00310.
19. Ali NI, Abidin SZZ, Majid SR. The high-performance polymer electrolytes based on agarose-$Mg(ClO_4)_2$ for application in electrochemical energy storage devices. J Adv Res Fluid Mech Therm Sci. 2024;118(1):65–85. doi:10.37934/arfmts.118.1.6585.
20. Khan NM, Kufian MZ, Samsudin AS. The correlation between SiO2 and the conduction properties of Li+ ions in an amorphous gel polymer electrolyte composed of PMMA/PLA-LiBOB. Res Sq. 2024;81(13):1–24. doi:10.21203/rs.3.rs-4410265/v1.
21. Polu AR, Kumar R, Rhee HW. Magnesium ion conducting solid polymer blend electrolyte based on biodegradable polymers and application in solid-state batteries. Ionics. 2015;21(1):125–32. doi:10.1007/s11581-014-1174-4.
22. Hussain NFS, Zainal Abidin SZ, Ahmad Shaharuddin NA, Raja Syiarizzad RNQA, Che Balian SR. Ionic transport and structural analysis of biopolymer electrolyte based on agarose integrated with sodium nitrate. Malay J Anal Sci. 2024;28(1):236–46.
23. Pradeep R, Siva V, Jothi MA, Murugan A, Shameem A, Sanjana S, et al. Structural, surface morphological and dielectric studies of guanidinium salt incorporated poly (ethylene oxide)/poly (vinyl pyrrolidone) solid polymer electrolytes. Heliyon. 2023;10(1):e23524. doi:10.1016/j.heliyon.2023.e23524.
24. Huang J, Gao Y, Luo J, Wang S, Li C, Chen S, et al. Editors' choice—review—impedance response of porous electrodes: theoretical framework, physical models and applications. J Electrochem Soc. 2020;167(16):166503. doi:10.1149/1945-7111/abc655.
25. Srinivasan MP, Punithavelan N. Investigation of electronic polarization-AC and DC conductivities of CeO_2/MnO_2 nanocomposite. J King Saud Univ Sci. 2022;34(4):101990. doi:10.1016/j.jksus.2022.101990.
26. Halizan MZ, Mohamed Z. Dielectric, AC conductivity, and DC conductivity behaviours of Sr2CaTeO6 double perovskite. Materials. 2022;15(12):4363. doi:10.3390/ma15124363.
27. Kumar S, Nagarajaiah SR, Raghu S, Dongre S, Thippaiah D, Jadiyappa S. Dielectric and conductivity study of salt-doped HPMC solid polymer electrolyte films. Biointerface Res Appl Chem. 2023;13(6):1–11. doi:10.33263/BRIAC136.529.
28. Yong J, Chen YC, Aziz SB, Khandaker MU, Woo HJ. Correlated barrier hopping dynamics of Na^+ ions in poly(vinyl alcohol) biopolymer-based solid polymer electrolytes: electrical and structural analysis. Electrochim Acta. 2025;513(4):145610. doi:10.1016/j.electacta.2024.145610.
29. Rajahmundry GK, Patra TK. Understanding ion distribution and diffusion in solid polymer electrolytes. Langmuir. 2024;40(36):18942–9. doi:10.1021/acs.langmuir.4c01543.
30. Kani Ajay Babu M, Jayabalakrishnan SS, Selvasekarapandian S, Aafrin Hazaana S, Meera Naachiyar R, Muniraj Vignesh N. Development and characterization of biopolymer electrolyte based on gellan gum for the fabrication of solid-state sodium-ion battery. Ionics. 2023;29(12):5249–65. doi:10.1007/s11581-023-05210-9.